Site-Specific Deuterium Order Parameters and Membrane-Bound Behavior of a Peptide Fragment from the Intracellular Domain of HIV-1 gp41

Bernd W. Koenig,[‡,§] James A. Ferretti,[||] and Klaus Gawrisch*[,‡]

Laboratory of Membrane Biochemistry and Biophysics, NIAAA, National Institutes of Health, 12420 Parklawn Drive, Room 158, Rockville, Maryland 20852, and Laboratory of Biophysical Chemistry, NHLBI, National Institutes of Health, Bethesda, Maryland 20892

Received November 30, 1998; Revised Manuscript Received March 17, 1999

ABSTRACT: The behavior of the cytolytic peptide fragment 828−848 (P828) from the carboxy-terminus of the envelope glycoprotein gp41 of HIV-1 in membranes was investigated by solid-state ^{2}H NMR on P828 with the selectively deuterated isoleucines I_3, I_{13}, I_{16}, and I_{20}. The quadrupole splittings of the I_3 side chain show significant sensitivity to the main phase-transition temperature of the lipid, consistent with partial penetration of the N-terminal peptide region into the hydrophobic core of the membrane. In contrast, the quadrupole splittings of I_{13}, I_{16}, and I_{20} are in agreement with a location of the C-terminal portion of the peptide near the lipid/water interface. The perturbation of the bilayer by the peptide was studied by ^{2}H NMR on *sn*-1 chain deuterated 1-stearoyl-2-oleoyl-*sn*-glycero-3-phosphoserine membranes. Peptide incorporation results in a significant reduction of lipid chain order toward the bilayer center, but only a modest reduction near the lipid glycerol. These observations suggest a penetration of the partially structured peptide backbone into the membrane/water interface region that reduces lateral packing density and decreases order in the hydrophobic core. In addition, the structure of the peptide was investigated free in water and bound to SDS micelles by high-resolution NMR. P828 is unstructured in water but exists in a flexible partially helical conformation when bound to negatively charged liposomes or micelles. The flexible helix covers the first 14 residues of the peptide, whereas the C-terminus of the peptide, where three of the six positively charged arginine residues are located, appears to be unstructured. The peptide-induced changes in lipid chain order profiles indicate that membrane curvature stress is the driving force for the cytolytic behavior of P828.

The investigated peptide, P828,[1] represents a 21 amino acid residue fragment of a putatively highly amphipathic region near the carboxy-terminal end of the envelope glycoprotein gp41 (residues 828−848) of human immunodeficiency virus Type I (HIV-1). The role of this amino acid segment of the C-terminal region of gp41 in viral replication and progression to disease is poorly understood, although it has been implicated in the cytotoxicity of the virus (*1*-*4*). Evidence for an interaction of gp41 with the viral membrane has been presented (*5*). Theoretical analysis indicated that, as an α-helix, P828 has an extraordinary high sequence hydrophobic moment (*6*−*8*). P828 also contains a relatively large number of positively charged amino acid residues. These features form the basis of the cytolytic properties of P828 (*9*, *10*). Furthermore, strong cytolytic effects on both prokaryotic and eukaryotic cells of a synthetic peptide, which is slightly longer than P828 (residues 828−855 of gp41), were demonstrated (*11*). The latter peptide alters membrane ionic permeability and induces cell lysis by formation of multimeric pores (*12*, *13*).

Amphipathic cytolytic peptides cause cell death by compromising the osmotic integrity of the cell membrane. Action occurs directly on the membrane and does not require involvement of membrane proteins. Examples of such peptides are antimicrobial host defense peptides (e.g., magainin (*14*)), certain venoms (e.g., melittin (*15*)), and the antibiotic peptide alamethicin from fungi (*16*). Binding of these peptides to membranes is frequently accompanied by the formation of amphipathic secondary structure elements (*14*). It has been shown that the overall structural organization of the folded peptide (e.g., hydrophobic moment (*17*); relative size of hydrophobic versus polar face (*18*); charge pattern (*12*)) is a critical feature for activity. Both electrostatic and hydrophobic interactions are involved in membrane binding (*19*). Some of these peptides, for example, host defense peptides, interact exclusively with negatively charged membranes, which may at least partially account for their specific action on microbial cells. Peptide binding induces changes in membrane morphology, which are lipid- and peptide-specific. Examples are the formations of conductive pores (*20*, *21*), discoidal micelles (*22*), or nonlamellar lipid phases

* Corresponding author. Phone: (301) 594-3750. Fax: (301) 594-0035. E-mail: gawrisch@helix.nih.gov.

‡ Laboratory of Membrane Biochemistry and Biophysics, NIAAA.

§ Current address: Technische Universität Darmstadt, Fachbereich Chemie, Institut für Biochemie, Darmstadt, Germany.

|| Laboratory of Biophysical Chemistry, NHLBI.

[1] Abbreviations: P828S, H_3N-RVIEVVQGASRAIRHIPRRIR-COOH; SOPS, 1-stearoyl-2-oleoyl-*sn*-glycero-3-phosphoserine; SDS, sodium dodecyl sulfate; NOE, nuclear Overhauser effect; NOESY, nuclear Overhauser enhancement spectroscopy; TOCSY, total correlation spectroscopy; ROESY, rotating-frame nuclear Overhauser enhancement spectroscopy; HSQC, heteronuclear single-quantum correlation; $R_{W/L}$, molar water-to-lipid ratio; $R_{L/P}$, molar lipid-to-peptide ratio.

10.1021/bi982800g
Published on Web 04/22/1999

(*23*, *24*). Either mechanism may contribute to a catastrophic increase in membrane permeability.

Understanding the cytolytic activity of P828 at a molecular level requires a comprehensive model of P828/membrane interaction. In particular, the membrane binding behavior of P828 (*25*) needs to be complemented with structural data on the membrane/peptide complex. The peptide binds strongly to negatively charged, but not to zwitterionic, liposomes (*25*). Binding is accompanied by a conformational transition of the peptide from being unstructured in solution to a predominantly helical structure in the membrane-bound state (*25*, *26*). The current study addresses three aspects of the interaction of P828 with membranes: (i) the depth of penetration of the peptide into the membrane; (ii) membrane perturbations caused by P828; and (iii) the conformation of the peptide in the bound state. The location of the peptide in the membrane was determined qualitatively from solid state ^{2}H NMR spectra of the four deuterated isoleucine side chains recorded as a function of the phase state of the lipid, and by investigation of the influence of peptide binding on order parameters of deuterated lipid hydrocarbon chains. The conformational transition of the peptide upon binding was studied by high-resolution NMR on the peptide in membrane mimetic SDS micelles and in aqueous solution.

EXPERIMENTAL PROCEDURES

Materials. The peptide P828S was synthesized by Peptide Technologies, Inc. (Gaithersburg, MD) using Fmoc solid-state synthesis protocols. Both protonated and selectively deuterated peptide, having the side chain of one of the four isoleucines perdeuterated (Cambridge Isotopes, Cambridge, MA), referred to as P828S-I$_x$-d10, with $x = 3$, 13, 16, or 20, were used. Peptide purity was higher than 95% as determined by both HPLC and electrospray mass spectrometry. The lipids 1-stearoyl-2-oleoyl-*sn*-glycero-3-phosphoserine (SOPS) and 1-stearoyl$_{d35}$-2-oleoyl-*sn*-glycero-3-phosphoserine (SOPS-d35) were obtained as sodium salts from Avanti Polar Lipids, Inc. (Alabaster, AL). Lipid integrity was verified by thin-layer chromatography.

The peptide analogue used in this study differs from the peptide P828 (amino acids 828−848 of gp41 of HIV isolate HXB2R (*27*)) by the presence of a serine rather than a cysteine in position 10 and is referred to as P828S. The cysteine residue is not conserved among different HIV isolates, and a variety of hydrophobic as well as polar, but electrically neutral, amino acids are found in this position (*27*).

Sample Preparation. For solid-state NMR, about 30 mg of lipid or of lipid and peptide were dispersed in buffer (150 mM NaCl, 10 mM MOPS, 1 mM EDTA in deuterium depleted water; pH adjusted to 7 using 0.1 M NaOH and HCl). Samples were thoroughly vortexed at ambient temperature and subjected to ultrasound for 3 × 1 min with intermittent vortexing to convert multilamellar liposomes into unilamellar lipid vesicles. This procedure exposes all lipids to the peptide. A Branson sonifier, model 250, equipped with a microtip was used. During sonication, the appearance of the solution changed from milky to opaque, indicating the break-up of large aggregates. Samples were ultracentrifuged at 400000*g* in a Beckmann TLX 100 benchtop centrifuge at 30 °C for 12 h. The lipid/peptide pellet was then transferred to thin-walled 5 mm glass tubes that were flame sealed. The amount of buffer in the lipid/peptide samples was estimated to be between 50 and 70 wt %. The absence of an isotropic signal in the ^{2}H and ^{31}P NMR lipid spectra confirmed that ultracentrifugation results in the formation of a homogeneous population of large multilamellar liposomes. The amount of peptide left in the supernatant was determined by UV/vis spectrophotometry. At least 95% of the peptide is bound in the pellet. The reported molar lipid/peptide ratios are accurate to ±10%.

Membranes that contain SOPS and the free amino acid isoleucine (I-d10) (molar ratio 4:1) were prepared from dispersions of lipid and I-d10 in deionized water at pH 7. The dispersions were combined and mixed by sonication and vortexing. The sample was lyophilized, rehydrated with buffer to give a molar water-to-lipid ratio ($R_{W/L}$) of 10, and homogenized by repeated backward and forward centrifugation.

For high-resolution NMR experiments, P828S (5.3 mM) was dissolved either in 90% H_2O/10% D_2O or in a 277 mM solution of perdeuterated sodium dodecyl sulfate (SDS-d25, Cambridge Isotopes, Cambridge, MA) in 90% H_2O/10% D_2O. The pH was adjusted to 3.5 and 4, respectively, by titration with 0.1 M NaOH and 0.1 M HCl. Samples were thoroughly vortexed and transferred to 5 mm NMR tubes (Shigemi Co. Ltd., Japan) utilizing an effective sample volume of 230 μL.

Solid-State NMR. ^{2}H and ^{31}P NMR spectra were recorded on a Bruker DMX300 spectrometer using a high-power probe with a 5 mm solenoid sample coil. The temperature was controlled to ±0.1 °C using a Bruker variable temperature unit. ^{2}H NMR spectra were acquired with a quadrupolar echo pulse sequence (*28*) at a 90° pulse length of 2.3 μs, a 50 μs delay between pulses, and a repetition rate of two acquisitions per second. A spectral width of 200 kHz was used for samples studied in the liquid-crystalline phase and a width of 500 kHz for samples in the gel or crystalline phases. Proton-decoupled ^{31}P NMR spectra (125 kHz spectral width) were recorded with a Hahn echo sequence at a 2.2 μs 90° pulse, a 40 μs delay between pulses, and a repetition rate of one acquisition per second.

Details on data processing have been published previously (*29*, *30*). Smoothed deuterium order parameter profiles of the lipid hydrocarbon chains were obtained from dePaked ^{2}H NMR powder pattern spectra (*31*−*33*). The projection length, *L*, of the perdeuterated lipid chain on the bilayer normal was calculated from the average order parameter, |S|, based on semiempirical models initially developed by Seelig et al. (*33*, *34*). The thickness of the hydrocarbon core of the membrane, d_{HC}, was assumed to be twice the average thickness of a monolayer, *L*. Lipid main phase-transition temperatures were determined from the temperature dependence of the ^{2}H NMR first spectral moment, M_1, that is known to decrease sharply at the gel to liquid-crystalline phase-transition of the lipid matrix (*28*).

High-Resolution NMR Studies of Peptide Structure. NMR spectra were recorded at both 50 and 60 °C on Bruker AMX600 (P828S in SDS) and DMX500 (P828S in water) spectrometers. Chemical shifts were referenced to the temperature-corrected chemical shift of water using 3-(trimethylsilyl) propionic acid as a standard. The resonance signal of water was attenuated by presaturation during the 2 s

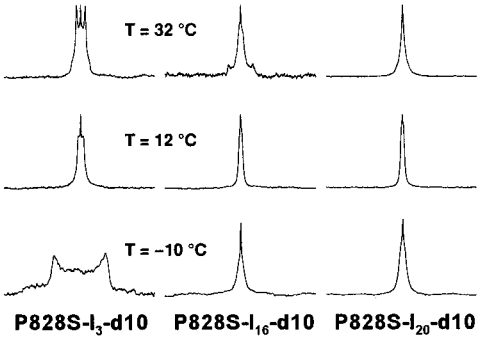

FIGURE 1: ^{2}H NMR powder pattern spectra of perdeuterated isoleucines inserted into the P828S sequence. Spectra are shown for SOPS/P828S-I_x-d10 mixtures with a molar ratio of 20:1 at 32 °C (top), 12 °C (middle), and −10 °C (bottom), respectively. The perdeuterated isoleucine was located at position I_3 (left), I_{16} (center), and I_{20} (right). Spectra obtained for perdeuterated isoleucine I_{13} (not shown) are similar to the spectra of I_{20}. A spectral range of 100 kHz is shown in all figures.

recycling delay and, for the NOESY experiment, also by saturation during the mixing time. For P828S in SDS-d25 micellar solution, two-dimensional total correlation spectroscopy (TOCSY) utilizing a WALTZ-17 spin-lock sequence (*35*, *36*) and 2D nuclear Overhauser effect spectroscopy (NOESY) experiments (*37*) with mixing times of 60 and 100 ms, respectively, were recorded with States quadrature detection in the indirect dimension (*38*). Data matrixes contained 512 increments in t_1 and 2048 increments in t_2, with 72 scans per t_1 increment for NOESY and 48 for TOCSY. Baseline correction of the time domain data was performed using the convolution method (*39*) to further suppress the residual water signal. A 90° shifted sine square bell window function was applied in both dimensions. Zero filling was used to obtain a digital resolution of 3 Hz in both dimensions. For P828S in water, 2D TOCSY and rotating-frame nuclear Overhauser enhancement spectroscopy (ROESY) (*40*) experiments with mixing times of 61 and 100 ms, respectively, were recorded using States-TPPI quadrature detection in the indirect dimension (*41*).

The ^{13}C chemical shifts of P828S in SDS-d25 micellar solution at 50 °C were determined by a gradient-enhanced 2D heteronuclear single-quantum correlation (HSQC) experiment (*42*) using a Bruker AMX600 spectrometer equipped with a triple-resonance 5 mm probehead containing a self-shielded z-gradient coil.

RESULTS

Isoleucine Side-Chain Order Parameters. ^{2}H NMR powder pattern spectra of four membrane-bound P828S analogues, each with one of the four isoleucine residues perdeuterated, were recorded at six temperatures covering the range from −10 to 32 °C. Samples at two molar SOPS-to-peptide ratios were studied; i.e., $R_{L/P} = 10$ and $R_{L/P} = 20$.

In the lipid gel phase (i.e., at −10° C), where the lipid hydrocarbon chains are packed in a crystalline lattice, the quadrupolar splitting of I_3 increases substantially compared to the liquid-crystal phase (i.e., at 32° C; Figure 1). This observation provides evidence for the penetration of I_3 into the membrane hydrophobic core. The splittings of the remaining three isoleucine resonances increase only marginally in going from the liquid-crystal to the gel phase, thereby

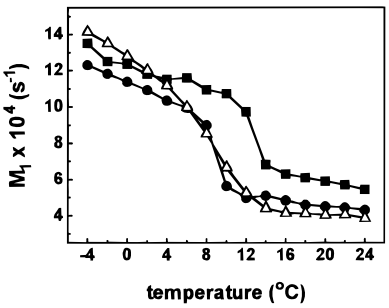

FIGURE 2: First moments, M_1, calculated from ^{2}H NMR spectra of SOPS-d35 are shown as a function of temperature. Data are presented for pure SOPS-d35 (■) and for samples with molar SOPS-d35/peptide ratios of 20:1 (●) and 10:1 (△).

suggesting a location of these isoleucines in the interface region. These measurements were carried out at a $R_{L/P} = 20$, since at the higher peptide concentration ($R_{L/P} = 10$), the apparent heterogeneity in peptide conformations in the gel phase is increased.

At 32 °C the ^{2}H NMR signal of I_3 shows one very well-resolved quadrupolar splitting of 6.7 kHz, I_{16} has two resolved splittings of 3.9 kHz and 17.4 kHz and a broadened central line, and I_{13} and I_{20} show this broadened central line only (Figure 1). NMR spectra of the deuterated side chains at $R_{L/P} = 10$ and $R_{L/P} = 20$ are similar. The quadrupolar splitting of I_3 is almost identical to the splitting of the free amino acid isoleucine incorporated into lipid bilayers, which also was measured as a control. The I_3 spectrum is characteristic of deep penetration of isoleucine into the bilayer, with the hydrophobic methyl groups located in the lipid hydrocarbon region and the polar peptide bond near the lipid/water interface. The spectra of I_{13}, I_{16}, and I_{20} have indications of inhomogeneous broadening that is characteristic of medium rate exchange between several environments with different order parameters. The most likely explanation for this observation is the presence of a set of peptide conformations that differ in the center and the C-terminal regions and undergo exchange at rates of up to 10^5 s^{-1}.

As the temperature is lowered through the phase transition (Figure 2), all peptide quadrupolar splittings first decrease and then increase again (Figure 1). The reduction in the quadrupolar splittings in the vicinity of the phase transition likely indicates an accumulation of P828S in the remaining fluid lipid domains. A locally higher peptide concentration results in more peptide disorder consistent with the observed lower splittings.

Influence of P828S on Lipid Hydrocarbon Order. The membrane remains in the lamellar phase upon binding of P828S even at the highest peptide concentration studied ($R_{L/P} = 10$), as indicated by the characteristic shape of the ^{31}P NMR powder pattern spectra. Peptide binding reduces the total breadth of the ^{2}H NMR powder pattern spectra in the L_α phase (Figure 3). This indicates a decrease in acyl chain order parameters, which are determined by a combination of influences involving average chain segment orientation and degree of orientational averaging. The ^{2}H NMR order parameter profiles (Figure 4) show the strongest decrease in chain order near carbon atom 11. We conclude that the decrease in order is more pronounced toward the center of the membrane compared to chain segments near the glycerol backbone of the lipid. The smaller magnitude of the peptide-

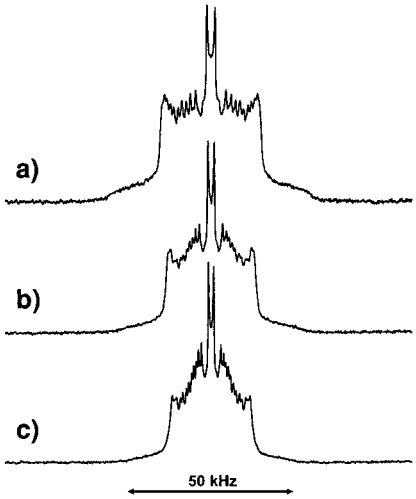

FIGURE 3: Influence of peptide P828S on ^{2}H NMR powder pattern spectra of SOPS-d35 at 32 °C. Spectra from SOPS-d35 without P828S (a) and with P828S at molar lipid/peptide ratios of 20:1 (b) and 10:1 (c), respectively, are presented.

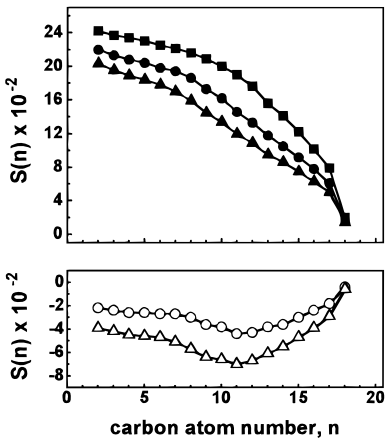

FIGURE 4: Influence of peptide P828S on the hydrocarbon chain order of SOPS-d35 at 32 °C. The ^{2}H NMR order parameter profiles of SOPS-d35 in the absence of P828S (■) and at molar lipid/peptide ratios of 20:1 (●) and 10:1 (▲), respectively, are shown in the upper panel. The peptide-induced difference in order parameters along the chain at molar lipid/peptide ratios of 20:1 (○) and 10:1 (△) is shown in the lower panel. Peptide-induced order changes are largest in the bilayer center, suggesting that the peptide acts as a spacer that is located in the membrane's interface region.

induced change in order parameters at the methyl end of the chain (Figure 4, bottom) is related to the very low order in this region. Deuterium order parameters are rather insensitive to perturbations of lipid chain order in the highly dynamic center of the membrane precluding interpretation of the difference order parameter profile close to the terminal methyl groups. The modest reduction in lipid order near the lipid/water interface in combination with the larger reduction in the bilayer center is indicative of a location of bound P828S within the bilayer near the lipid/water interface. Similar changes in lipid order were observed for anesthetics (*43*) and tryptophan analogues (*44*) that are also located in the interface region.

The P828S-induced decrease in chain order also indicates a reduction of the hydrocarbon core thickness of the membrane (*30*). The effect is concentration-dependent and amounts to about 1 Å at $R_{L/P} = 20$ and about 2 Å at $R_{L/P} =$

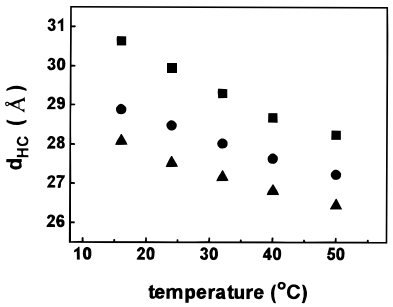

FIGURE 5: Influence of peptide P828S on the thickness of the hydrocarbon core, d_{HC}, of SOPS-d35 membranes in the liquid-crystalline phase as a function of temperature. Data were calculated for SOPS-d35 in the absence of P828S (■) and for samples with molar lipid/peptide ratios of 20:1 (●) and 10:1 (▲), respectively, as described in the text.

10 (Figure 5). The observed membrane thinning is not peculiar for binding of P828S to membranes. It appears to be a general consequence of peptide incorporation into the polar membrane region. Membrane thinning has been observed previously by X-ray diffraction on alamethicin- (*45*) and magainin-containing bilayers (*46*).

Incorporation of P828S into SOPS-d35 membranes lowers the temperature of the main phase transition of the lipid as measured by ^{2}H NMR (Figure 3). The spectra recorded in the phase-transition region represent a superposition of fluid and gel lipid domains. The amount of lipid in these domains varies with temperature. Only one set of lipid quadrupolar splittings is observed for the fluid domains, suggesting that SOPS/P828S complexes are short-lived on the ^{2}H NMR time scale of 10^{-5} s. Peptide binding lowers the phase-transition midpoint by about 3 °C at $R_{L/P}$ values of both 20 and 10. Lower phase-transition temperatures indicate a preferential interaction of P828S with the fluid lipid phase. Significant broadening of the phase transition is observed at $R_{L/P} = 10$, but not at $R_{L/P} = 20$. The broadening could be linked to differences in the process of peptide redistribution into fluid lipid domains at the phase transition.

Conformational Behavior of P828S from High-Resolution NMR. For P828S in water, most of the backbone proton resonances were unequivocally assigned at both 50 and 60 °C. No preference for any particular structure is found when screening the αH proton chemical shift values by using the shift index method (*47*). Sequential NH/NH (i, $i + 1$) NOE connectivities are completely absent in the ROSY spectra, and the temperature coefficients of the NH proton chemical shifts span a rather narrow range of $-(6 \pm 2)$ ppb/K (Figure 8b), confirming the lack of α-helical structure.

For P828S in the presence of SDS micelles, all backbone and most side-chain proton resonances were unequivocally assigned from the two-dimensional TOCSY and NOESY spectra. Interaction with SDS micelles results in conformational changes in the peptide that are reflected in the NOE connectivity pattern and in chemical shift changes of most backbone proton and some of the side-chain proton resonances. NOE connectivities observed for P828S in SDS micellar solution at 50 °C are summarized in Figure 6. The data suggest the existence of a helical stretch extending from V_2 or I_3 to R_{14}. The measured ratio between the average intensity of all NH/NH (i, $i + 1$) and αH/NH (i, $i + 1$) NOE cross-peaks at 50 °C is 1.7. An intensity ratio of 3.8, 5, or 0.02 would be expected for an α-helix, a 3_{10}-helix, or a

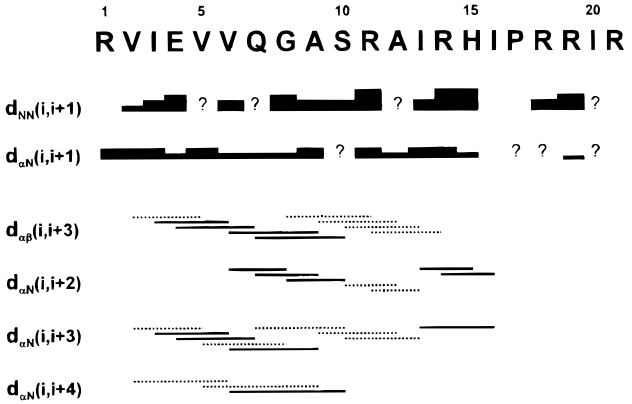

FIGURE 6: Summary of observed ^{1}H-^{1}H NOE connectivities from 2D NOESY spectra of P828S in SDS-d25 solution at 50 °C. For NH(i)/NH(i + 1) and for αH(i)/NH(i + 1) cross-peaks, the height of the boxes is proportional to the estimated NOE intensities. Question marks indicate cross-peaks that cannot be assessed due to signal overlap. Medium-range NOE interactions are summarized in the four lower rows. Solid bars indicate unique cross-peaks, while dotted lines are used for connectivities whose presence or absence cannot be assessed due to spectral overlap. Observation of medium-range cross-peaks of the peptide region near the C-terminus was not possible due to the proximity of the corresponding αH resonances to water. According to induced changes in chemical shift, this region is unstructured.

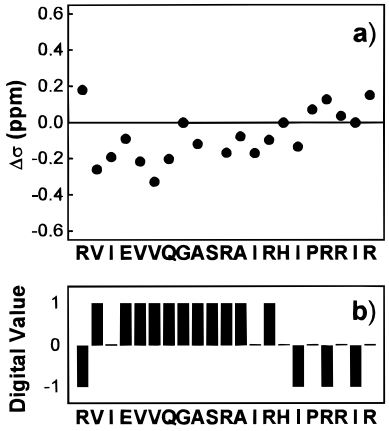

FIGURE 7: Map of chemical shift changes of P828S in SDS micellar solution at 50 °C. (a) Conformation-induced chemical shift of the αH backbone resonances. Shown is the difference between the chemical shift values observed in water and in SDS solution. (b) Digital values of the α^{13}C conformation-induced resonance shifts of the peptide (see Results section and ref *52*). The data confirm the existence of a helical stretch from V_2 to R_{14}.

β-sheet, respectively, on the basis of the geometry of these conformations (*48*). The observed ratio suggests that P828S is a flexible helix (*49*) that exists in at least two or, perhaps, a set of different conformations in rapid exchange. Helicity was evaluated also by induced changes of αH and α^{13}C chemical shift values (*50*, *51*) as shown in Figure 7. All but two αH resonances in the stretch from V_2 to I_{16} experience an upfield shift in SDS solution, thus suggesting formation of a helical structure. The α^{13}C chemical shift values have been compared with statistical averages for each amino acid in proteins and are categorized into values of +1, 0, and −1 (*52*). The stretch of mostly +1 values from V_2 to R_{14} suggests the existence of a helical conformation in this region of P828S. There is no evidence for helical structure in the C-terminal end of P828S. In micelle-bound P828S, the peptide bond between I_{16} and P_{17} adopts the trans conformation on the basis of the observation of NOESY cross-peaks between the αH proton of I_{16} and the δCH_2 protons of P_{17}, and between the amide NH proton of I_{16} and δCH_2 of P_{17} (*48*).

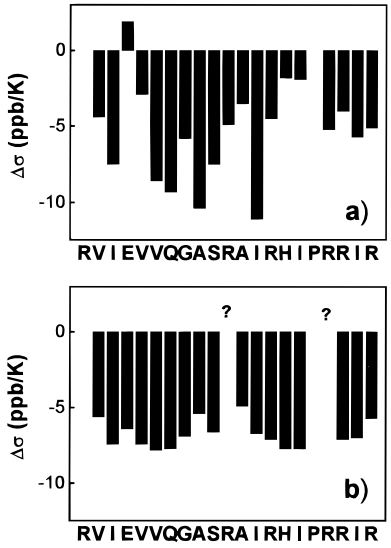

FIGURE 8: Temperature dependence of P828S amid proton chemical shifts in SDS micellar solution (a) and in water (b). The temperature coefficients are reported in parts per billion, per Kelvin. The variations in temperature coefficients along the peptide chain in SDS micelles are the result of helix formation and of peptide immersion into micelles.

The NH proton temperature coefficients of P828S in SDS micellar solution cover a wide range of values from −11 to +2 ppb/K for I_{13} and E_4, respectively (Figure 8). Small temperature coefficients between 0 and −3 ppb/K are typical for rigid secondary structure elements that are stabilized by intramolecular hydrogen bonds (*53*). Large temperature coefficients result from conformational flexibility of the peptide. The wide dispersion of temperature coefficients may indicate some conformational flexibility. Furthermore, an interfacial location of the peptide may also result in dispersion of temperature coefficients, since hydration of individual amide protons may vary significantly. We have no conclusive explanation for the rather unusual positive value of the temperature coefficient observed for E_4.

DISCUSSION

Locating peptides or protein fragments in membranes and determining their structure in the bound state have been the subject of considerable effort in recent years (*54*−*56*). The high degree of molecular disorder in liquid-crystalline membranes makes such investigations challenging. NMR studies, in combination with specific deuterium labeling of both the peptide and the lipid, are particularly useful since they permit an investigation of the motional behavior in specific positions of the peptide sequence together with a membrane depth-specific study of the related perturbation in lipid order. In the present study, we use a combination of solid-state and high-resolution NMR techniques to establish a link between peptide incorporation, the corresponding changes in the lipid matrix, and peptide structure.

Incorporation of P828S into the Membrane Interface. The ^{2}H NMR quadrupole splittings of P828S, with specifically deuterated isoleucines, and the SOPC-d35 chain order

parameters suggest substantial peptide penetration into the membrane interface. Conclusions regarding location of the N-terminal region of the peptide were derived from the quadrupole splitting of the I_3 side chain. The spectra of this amino acid are almost identical to the spectra of free perdeuterated isoleucine that was incorporated into the hydrocarbon region of the lipid matrix. When the lipid converts to the gel state, the order parameter of I_3 increases together with the order of lipid hydrocarbon chains. Therefore, we conclude that the N-terminal region of P828S is deeply immersed into the membrane interface. This location provides an environment of low dielectric constant and diminished water activity that favors the formation of intramolecular peptide hydrogen bonds (*57*) and is consistent with the tendency to adopt a helical conformation.

The ^{2}H NMR spectra of I_{13}, I_{16}, and I_{20}, which are located in the central and C-terminal portions of P828S, show some heterogeneity in their quadrupolar splittings and, on average, lower order parameters when compared with that of I_3. The side chains of residues I_{13}, I_{16}, and I_{20} do not show any additional broadening from the crystalline-like environment of the gel phase of the lipid, excluding side-chain location in the hydrophobic core. Below the phase transition, in the lipid L_β phase, only the lipid hydrocarbon chains are packed in a crystalline lattice, while the lipid headgroups remain rather mobile. Therefore, the gel-phase quadrupole splittings of I_{13}, I_{16}, and I_{20} are in agreement with a more shallow incorporation of the peptide C-terminal portion into the polar lipid headgroup region.

Supporting evidence for locating the P828 backbone in the lipid/water interface comes from binding studies of antibodies that react specifically with carboxy-terminal fragments of gp41. An antibody raised against amino acid residues 839−853 of gp41 is incapable of binding to its target sequence when gp41 is bound to microsomes (*5*). This inability to bind implies that the cytoplasmic tail of gp41 is tightly associated with the microsomal membrane. Furthermore, the interaction of P828 with lipid monolayers at the air/water interface also demonstrates penetration of the peptide into the monolayer (*58*).

Structure of Membrane-Bound P828S. High-resolution NMR investigations indicate a transition of P828S from an unstructured state in water to a conformation with a high degree of helical content upon binding to SDS micelles. CD spectra of P828 in micellar solution are identical to spectra of P828 bound to negatively charged liposomes, suggesting that the structure of the peptide is very similar in both cases (*25*, *26*). The NMR cross-peak pattern of P828S in the SDS-bound state, and the differences in chemical shift of peptide backbone resonances between water and SDS solution, confirm the existence of a flexible helical stretch covering residues 2−14. The remainder of the molecule, which includes three of the six positively charged arginines of P828S, appears to be unstructured. The absence of secondary structure in the C-terminal region of the peptide correlates well with the structural heterogeneity that is observed in the quadrupole splittings of deuterated isoleucines I_{13}, I_{16}, and I_{20} of membrane-bound P828S. This lends further support to the hypothesis that the peptide has the same structure in the lipid bilayer and in SDS micelles.

It was calculated that, as a regular α-helix, P828 has a very high sequence hydrophobic moment (*7*) with a maximum of amphipathic character at the peptide C-terminus. In the amphipathic α-helix, the positively charged arginine side chains are located at the hydrophilic face while the isoleucines are in the hydrophobic face. Placing this hypothetical structure in the water near the membrane would account for the electrostatic interaction between peptide and lipid, but it would also expose the hydrophobic peptide face to water (*25*, *59*). In contrast to this model, we found that P828S is deeply immersed into the lipid/water interface, with a helical region in the N-terminal half that is flexible, and a C-terminal region that has no distinct secondary structure. The NMR results do not support the hypothesis that P828 forms a well-defined amphipathic α-helix in the membrane-bound state. Therefore, a structural analysis that emphasizes the location of peptide side chains on a specific helical face is inappropriate. Also, the location of P828 in the bilayer interface makes the need for locating specific side chains at distinct faces of P828 less obvious, because this interface is characterized by a fair amount of molecular disorder.

Mechanism of Membrane Binding. The major driving force for P828S binding to membranes, and for helix formation, is the attractive electrostatic interaction between the negatively charged lipid headgroups and the positively charged arginine side chains of P828S (*25*). Penetration of the N-terminal portion of P828S into the membrane/water interface suggests an additional gain in free energy due to the hydrophobic effect. However, binding of P828 to zwitterionic lipids is not detectable (*25*) or is very weak (*58*), thus indicating that hydrophobic interactions alone are insufficient to yield significant membrane−peptide association. The peptide adopts a helical structure in media of reduced polarity such as methanol (*25*) or aqueous TFE solutions (*26*), but attempts to induce helix formation by neutralization of the peptide charges in aqueous solution with high ionic strength (*25*) or pH titration (*26*) were not successful. Therefore, we conclude that the structural transition from disordered (in solution) to helical (in the membrane-bound state) is a direct consequence of the immersion of P828S into the less polar environment of the membrane interface.

P828S-Induced Membrane Perturbation. The perturbation of SOPS chain order is caused by the insertion of the peptide backbone into the membrane interface. It acts as a spacer that laterally separates the lipid hydrocarbon chains. In the interface region, the peptide fills most of the extra volume, but the lipid methylene segments that are further away from the interface have a larger volume to move into and are disordered to a greater extent (Figure 4).

It was previously suggested that a nonuniform change of order parameters along the lipid hydrocarbon chains is an indication for alterations in the lateral pressure profile of the membrane (*60*−*62*). Indeed, the differences in distance between lipid segments as a result of peptide incorporation into the membrane/water interface are likely to alter lateral forces within the bilayer. In particular, it can be expected that lateral repulsion between lipid molecules in the hydrophobic core is lower. In contrast, repulsion close to the glycerol remains unchanged or decreases to a lesser extent. This asymmetry in the lateral forces along the lipid monolayer normal results in positive curvature stress (*63*) that could lead to pore formation and, thus, provides a basis for the understanding of cytolytic activity.

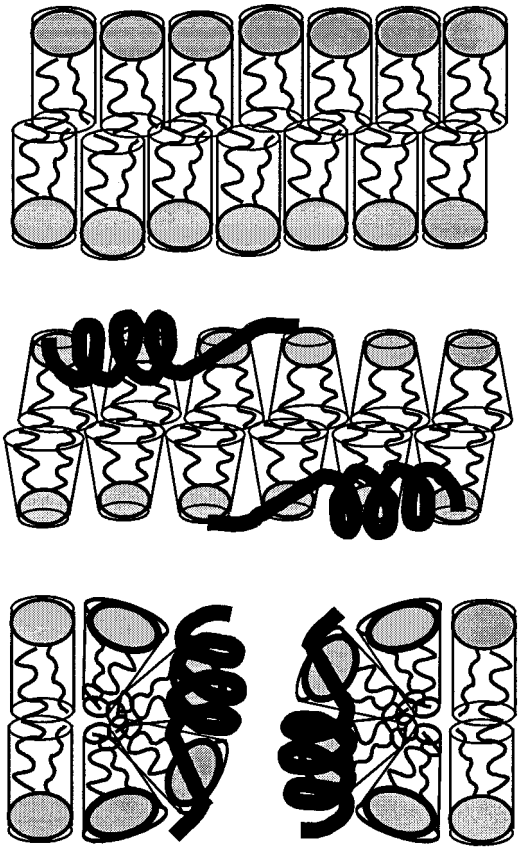

FIGURE 9: Cartoon showing the location of membrane-bound peptide P828S and its influence on packing of lipid molecules. Without peptide the lipids pack with cylindrical symmetry (top). Interfacial binding of P828S increases mobility of lipid hydrocarbon chains in the center of the membrane, indicating the existence of membrane curvature stress that drives lipid headgroups apart (middle). Membrane curvature stress gets released upon the formation of lipidic pores, which are collectively lined by lipid headgroups and peptide molecules (bottom).

Implications for Cytolytic Activity of P828S. Two aspects of peptide/membrane interaction are crucial for establishing cytolytic activity: (i) recruitment of the peptide to the membrane by electrostatic interactions, and (ii) cell membrane lysis or pore formation that results in complete breakdown of ionic gradients, or a Ca^{2+}-influx that triggers apoptosis. Binding of P828 to the SOPS membrane results in monolayer curvature stress. As discussed in a recent paper by Matsuzaki et al. (*64*) for the peptide magainin 2, the formation of toroidal pores depends on two types of membrane curvature, positive curvature that is related to the pore length and negative curvature that is related to the pore diameter. While the free energy of narrow pores has contributions from both positive and negative membrane curvature, the free energy of wide pores is dominated by the positive curvature term. At high P828/lipid molar ratios, pores with large diameters have been observed (*12*, *65*). Therefore, P828-induced pore formation is most likely the result of positive curvature stress from peptide binding. The positive curvature in the pore lining favors some degree of transmembrane orientation of P828.

Conductance measurements indicated cationic selectivity of the pores, implying a negative net charge of the channel lining (*65*). We propose that the lipid/peptide organization in the pore lining is similar to that of lamellar lipid/peptide complexes (Figure 9). The penetration of the peptide into the interface satisfies the amphipathic character of the peptide, and the presence of lipid headgroups in the pore lining provides for peptide charge neutralization, thus preventing a pore-destabilizing positive net charge (*19*). In BLM experiments, a P828 concentration of at least 2 μM was required to trigger pore formation (*65*). At this concentration, on the order of 2×10^{13} peptide molecules are bound per square centimeter of lipid monolayer, corresponding to a lipid/peptide ratio $R_{L/P} = 8$. At P828 concentrations of $R_{L/P} \geq 10$, the peptide locates predominantly in the bilayer/water interface without pore formation, which is in agreement with our spectroscopic results.

The concentration-dependent partial translocation from the membrane interface to transmembrane pores appears to be a general feature in the action of amphipathic cytolytic peptides, including P828S. For example, alamethicin and magainin are oriented parallel to the membrane surface at a low peptide/lipid ratio but completely insert in a transmembrane orientation at high peptide concentration with a transition region at intermediate concentrations (*66*, *67*). The changes in lipid order profiles suggest that membrane curvature stress is the driving force for peptide translocation and pore formation.

ACKNOWLEDGMENT

We thank Dr. S. König for checking peptide purity with electrospray mass spectrometry and Prof. S. Grzesiek for running the HSQC experiment.

REFERENCES

1. Fisher, A. G., Ratner, L., Mitsuya, H., Marselle, L. M., Harper, M. E., Broder, S., Gallo, R. C., and Wong-Staal, F. (1986) *Science 233*, 655−659.
2. Hirsch, V., Riedel, N., and Mullins, J. I. (1987) *Cell 49*, 307−319.
3. Lee, S. J., Hu, W., Fisher, A. G., Looney, D. J., Kao, V. F., Mitsuya, H., Ratner, L., and Wong-Staal, F. (1989) *AIDS Res. Hum. Retroviruses 5*, 441−449.
4. Gabuzda, D. H., Lever, A., Terwilliger, E., and Sodroski, J. (1992) *J. Virol. 66*, 3306−3315.
5. Haffar, O. K., Dowbenko, D. J., and Berman, P. W. (1988) *J. Cell Biol. 107*, 1677−1687.
6. Venable, R. M., Pastor, R. W., Brooks, B. R., and Carson, F. W. (1989) *AIDS Res. Hum. Retroviruses 5*, 7−22.
7. Eisenberg, D., and Wesson, M. (1990) *Biopolymers 29*, 171−177.
8. Eisenberg, D., Wesson, M., and Wilcox, W. (1989) in *Prediction of protein structure and the principles of protein conformation* (Fasman, G. D., Ed.) pp 635−646, Plenum Press, New York.
9. Kaiser, E. T., and Kezdy, F. J. (1987) *Annu. Rev. Biophys. Biophys. Chem. 16*, 561−581.
10. Miller, M. A., and Montelaro, R. C. (1992) in *Membrane interactions of HIV: Implications for pathogenesis and therapy in AIDS* (Aloia, R. C., Curtain, C. C., Eds.) pp 351−364, Wiley-Liss, New York.
11. Miller, M. A., Garry, R. F., Jaynes, J. M., and Montelaro, R. C. (1991) *AIDS Res. Hum. Retroviruses 7*, 511−519.
12. Miller, M. A., Cloyd, M. W., Liebmann, J., Rinaldo, C. R., Islam, K. R., Wang, S. Z. S., Mietzner, T. A., and Montelaro, R. C. (1993) *Virology 196*, 89−100.
13. Comardelle, A. M., Norris, C. H., Plymale, D. R., Gatti, P. J., Choi, B., Fermin, C. D., Haislip, A. M., Tencza, S. B., Mietzner, T. A., Montelaro, R. C., and Garry, R. F. (1997) *AIDS Res. Hum. Retroviruses 13*, 1525−1532.

14. Maloy, W. L., and Kari, U. P. (1995) *Biopolymers 37*, 105−122.
15. Dempsey, C. E. (1990) *Biochim. Biophys. Acta 1031*, 143−161.
16. Cafiso, D. S. (1994) *Annu. Rev. Biophys. Biomol. Struct. 23*, 141−165.
17. Wieprecht, T., Dathe, M., Krause, E., Beyermann, M., Maloy, W. L., MacDonald, D. L., and Bienert, M. (1997) *FEBS Lett. 417*, 135−140.
18. Wieprecht, T., Dathe, M., Epand, R. M., Beyermann, M., Krause, E., Maloy, W. L., MacDonald, D. L., and Bienert, M. (1997) *Biochemistry 36*, 12869−12880.
19. Bechinger, B. (1997) *J. Membr. Biol. 156*, 197−211.
20. Matsuzaki, K., Murase, O., Fujii, N., and Miyajima, K. (1996) *Biochemistry 35*, 11361−11368.
21. Ludtke, S. J., He, K., Heller, W. T., Harroun, T. A., Yang, L., and Huang, H. W. (1996) *Biochemistry 35*, 13723−13728.
22. Dufourcq, J., Faucon, J.-F., Fourche, G., Dasseux, J.-L., LeMaire, M., and Gulik-Krzywicki, T. (1986) *Biochim. Biophys. Acta 859*, 33−48.
23. Batenburg, A. M., and deKruijff, B. (1988) *Biosci. Rep. 8*, 299−307.
24. Batenburg, A. M., Hibbeln, J. C. L., and deKruijff, B. (1987) *Biochim. Biophys. Acta 903*, 155−165.
25. Gawrisch, K., Han, K.-H., Yang, J.-S., Bergelson, L. D., and Ferretti, J. A. (1993) *Biochemistry 32*, 3112−3118.
26. Koenig, B. W., Bergelson, L. D., Gawrisch, K., Ward, J., and Ferretti, J. A. (1995) *Mol. Membr. Biol. 12*, 77−82.
27. Myers, G., Korber, B., Foley, B., Jeang, K.-T., Mellors, J. W., and Wain-Hobson, S. (1996) *Human retroviruses and AIDS 1996: A compilation and analysis of nucleic acid and amino acid sequences*, Los Alamos National Laboratory, Los Alamos, NM.
28. Davis, J. H. (1983) *Biochim. Biophys. Acta 737*, 117−171.
29. Holte, L. L., Peter, S. A., Sinnwell, T. M., and Gawrisch, K. (1995) *Biophys. J. 68*, 2396−2403.
30. Koenig, B. W., Strey, H. H., and Gawrisch, K. (1997) *Biophys. J. 73*, 1954−1966.
31. Sternin, E., Bloom, M., and MacKay, A. L. (1983) *J. Magn. Reson. 55*, 274−282.
32. Lafleur, M., Fine, B., Sternin, E., Cullis, P. R., and Bloom, M. (1989) *Biophys. J. 56*, 1037−1041.
33. Seelig, A., and Seelig, J. (1974) *Biochemistry 13*, 4839−4845.
34. Schindler, H., and Seelig, J. (1975) *Biochemistry 14*, 2283−2287.
35. Bax, A., and Davis, D. G. (1985) *J. Magn. Reson. 65*, 355−360.
36. Bax, A. (1989) *Methods Enzymol. 176*, 151−168.
37. Kumar, A., Ernst, R. R., and Wüthrich, K. (1980) *Biochem. Biophys. Res. Commun. 95*, 1−6.
38. States, D. J., Haberkorn, R. A., and Ruben, D. J. (1982) *J. Magn. Reson. 48*, 286−292.
39. Marion, D., Ikura, M., and Bax, A. (1989) *J. Magn. Reson. 84*, 425−430.
40. Bothner-By, A. A., Stephens, R. L., Lee, J., Warren, Ch. D., and Jeanloz, R. W. (1984) *J. Am. Chem. Soc. 106*, 811−813.
41. Marion, D., Ikura, M., Tschudin, R., and Bax, A. (1989) *J. Magn. Reson. 85*, 393−399.
42. Kay, L. E., Keifer, P., and Saarinen, T. (1992) *J. Am. Chem. Soc. 114*, 10663−10665.
43. Boulanger, Y., Schreier, S., and Smith, I. C. P. (1981) *Biochemistry 20*, 6824−6830.
44. Yau, W. M., Wimley, W. C., Gawrisch, K., and White, S. H. (1998) *Biochemistry 37*, 14713−14718.
45. Wu, Y., He, K., Ludtke, S. J., and Huang, H. W. (1995) *Biophys. J. 68*, 2361−2369.
46. Ludtke, S. J., He, K., and Huang, H. W. (1995) *Biochemistry 34*, 16764−16769.
47. Wishart, D. S., Sykes, B. D., and Richards, F. M. (1992) *Biochemistry 31*, 1647−1651.
48. Wüthrich, K. (1986) *NMR of proteins and nucleic acids*, John Wiley & Sons, New York.
49. Dyson, H. J., and Wright, P. E. (1991) *Annu. Rev. Biophys. Biophys. Chem. 20*, 519−538.
50. Wishart, D. S., Sykes, B. D., and Richards, F. M. (1991) *J. Mol. Biol. 222*, 311−333.
51. Spera, S., and Bax, A. (1991) *J. Am. Chem. Soc. 113*, 5490−5492.
52. Wishart, D. S., and Sykes, B. D. (1994) *J. Biomol. NMR 4*, 171−180.
53. Deslauriers, R., and Smith, I. C. P. (1980) in *Biological Magnetic Resonance* (Berliner, L. J., Reuben, J., Eds.) Vol. 2, pp 243−344, Plenum Press, New York.
54. Ketchem, R. R., Hu, W., and Cross, T. A. (1993) *Science 261*, 1457−1460.
55. Dempsey, C. E., and Watts, A. (1987) *Biochemistry 26*, 5803−5811.
56. Keniry, M. A., Gutowsky, H. S., and Oldfield, E. (1984) *Nature 307*, 383−386.
57. Engelman, D. M. (1996) *Science 274*, 1850−1851.
58. Trommeshauser, D., and Galla, H. J. (1998) *Chem. Phys. Lipids 94*, 81−96.
59. Gawrisch, K., Barry, J. A., Holte, L. L., Sinnwell, T., Bergelson, L. D., and Ferretti, J. A. (1995) *Mol. Membr. Biol. 12*, 83−88.
60. Harries, B., and Ben-Shaul, A. (1997) *J. Chem. Phys. 106*, 1609−1619.
61. Cantor, R. S. (1997) *J. Phys. Chem. B 101*, 1723−1725.
62. Cantor, R. S. (1997) *Biochemistry 36*, 2339−2344.
63. Epand, R. M., Shai, Y., Segrest, J. P., and Anantharamaiah, G. M. (1995) *Biopolymers 37*, 319−338.
64. Matsuzaki, K., Sugishita, K., Ishibe, N., Ueha, M., Nakata, S., Miyajima, K., and Epand, R. M. (1998) *Biochemistry 37*, 11856−11863.
65. Chernomordik, L., Chanturiya, A. N., Suss-Toby, E., Nora, E., and Zimmerberg, J. (1994) *J. Virol. 68*, 7115−7123.
66. He, K., Ludtke, S. J., Heller, W. T., and Huang, H. W. (1996) *Biophys. J. 71*, 2669−2679.
67. Ludtke, S. J., He, K., Wu, Y., and Huang, H. W. (1994) *Biochim. Biophys. Acta 1190*, 181−184.

BI982800G